11

Universal Quantification of Chemical Bond Strength and Its Application to Low Dimensional Materials

Bo Xu, Xiaoju Guo and Yongjun Tian
State Key Laboratory of Metastable Materials Science and Technology
Yanshan University, Qinhuangdao, Hebei 066004
China

1. Introduction

The chemical bond strength describes the ability of a chemical bond holding two constituting atoms together. Many physical and mechanical properties of a material, such as melting point, activation energy of phase transition, tensile and shear strength, and hardness, are closely related to the bond strength (Kittle, 2004). However, a universal quantification of bond strength in crystal is hard to be performed due to the lack of effective microscopic parameters to characterize the bond strength. Usually, different characteristic parameters are chosen for different materials. For simple substances and covalent compounds, bond strength is correlated to cohesive energy. For ionic crystals, breaking a chemical bond means overcoming of the electrostatic interaction between anion and cation, which is defined as lattice energy and used to characterize bond strength. Correspondingly, several theoretical definitions of chemical bond strength have been proposed, such as Pauling's definition for ionic crystals (Pauling, 1929), orbital scaling for covalent crystals (Hultgren, 1932), and two power-law expressions for a variety of materials (Brown & Shannon, 1973; Gibbs et al., 2003). These definitions of bond strength are only valid for some specific types of crystals, and a generalized model of bond strength has not been reached.

In a crystal, bond strength is an intrinsic property of chemical bond, and is regulated by the constitutional atoms as well as the crystal structure. From this viewpoint, bond strength is directly determined by the bond length and the shared bonding electrons. Obviously, greater bond strength would be expected with shorter bond length. The extent of electron sharing, related to the electronegativity difference of bond-forming atoms, is determined by the localized electron density in the binding region. It was found that the greater the localized electron density, the more the effective bonding electrons, and the stronger the bond strength (Gibbs et al., 2003). Most recently, we established a universal semi-empirical quantitative scale to describe the strength of chemical bond in crystals (Guo et al., 2009). The chemical bond strength is defined as the maximum force that a chemical bond can resist under the uniaxial tension along the bond direction which is called tensile unbinding force. We found that the bond strength only relies on two parameters, the bond length and effectively bonded valence electron number of a chemical bond.

In the following, the concept of effectively bonded valence electron number of chemical bond is introduced and the universal quantification model of chemical bond strength is established based on effectively bonded valence electron number and bond length exclusively. The correlation between ideal tensile strength and chemical bond strength is presented. This model allows a convenience determination of chemical bond strength for a variety of materials, ranging from covalent crystals to ionic crystals as well as low dimensional materials. Its application to low dimensional materials, such as graphene, h-BN sheet, and SWNT, are also presented.

2. Methodology

As mentioned in the introduction, the shared bonding electrons in the binding region of two bonded atoms plays a vital role in determining the bond strength. To establish an effective quantification model of bond strength, we must find a practical way to estimate the population of these electrons.

Considering two atoms, A and B, forming a bond in a crystal, the valence electrons are Z_A and Z_B with coordination numbers of N_A and N_B, respectively. We first consider a simple case where bonded atom pair possesses totally eight valence electrons. The nominal valence electrons contributed to the A-B bond are $n_A = Z_A/N_A$ and $n_B = Z_B/N_B$ from atom A and B, respectively. Larger localized electron density in the binding region would result in stronger bond. However, the bonded electrons localized in the binding region are basically smaller than n_A or n_B. The Mulliken overlap population of a bond from first-principles calculations can provide a measurement of the bonded electrons (Mulliken, 1955). For example, the calculated population is 0.75 for C-C bonds in diamond and 0.19 for Na-Cl bonds in NaCl crystal. While the determination of population greatly depends on the calculation formalisms (Segall et al., 1996), it is more convenient to find a parameter, which can be easily determined, to serve as an alternative population. Here we propose the effectively bonded valence electron (EBVE) number, n_{AB}, of A-B bond in terms of n_A and n_B as

$$n_{AB} = \frac{n_A n_B}{\sqrt{n_A^2 + n_B^2}} \tag{1}$$

The EBVE numbers of diamond (0.707) and NaCl (0.163) are in good agreement with the Mulliken population. Some EBVE numbers of various covalent and ionic crystals are listed in our previous publication (Guo et al., 2009) as well as in the following text.

The ideal A-B bond strength can essentially be defined as an unbinding force of chemical bond, and the physical feature of bond strength for solids becomes more apparent and more accessible than Pauling's definition or other above-mentioned energy scales. Previously, the power-law behavior of the bond length on bond strength are suggested (Brown & Shannon, 1973; Gibbs et al., 1998, 2003), and the exponential dependence of the resistance of a bond to indenter on the population-related ionicity is emphasized (Gao et al., 2003; He et al., 2005; Li et al., 2008; Simunek & Vackar, 2006). These studies have highlighted the role of the bond length and valance electrons on the strength of a chemical bond. The chemical bond strength, defined as the tensile unbinding force F_{AB}, can then be described quantitatively in terms of the bond length d_{AB} and EBVE number n_{AB} with the formalism,

$$F_{AB} = Cd_{AB}^{-m}\exp(kn_{AB}) \tag{2}$$

where constants C, m, and k can be deduced from first-principles calculations.

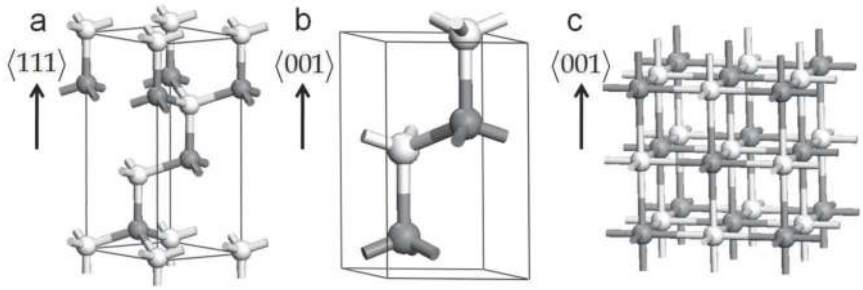

Fig. 1. Typical crystal structures of a) zincblende, b) wurtzite, and c) rock salt with the weakest tensile directions marked.

As soon as the tensile unbinding force of a bond is known, the ideal tensile strength of a crystal is easily accessible. For simple structural crystals shown in Figure 1, generally, the weakest tensile directions, such as $\langle 111 \rangle$ of zincblende (ZB), $\langle 001 \rangle$ of wurtzite (WZ), and $\langle 001 \rangle$ of rock salt (RS) structures, are parallel to the axes of the bonds to be broken. Thus, the ideal tensile strength, σ_{hkl}, of a crystal along the weakest $\langle hkl \rangle$ direction should be correlated with F_{AB} through

$$\sigma_{hkl} = S_{hkl}F_{AB} = CS_{hkl}d_{AB}^{-m}\exp(kn_{AB}) \tag{3}$$

where S_{hkl} in the unit of m^{-2} is the number of the broken bonds per unit area on the (hkl) plane, which has the lowest bond density.

Alternatively but more time-consumingly, the ideal tensile strength of a crystal can be determined from first-principles calculations (Roundy et al., 1999). We acquired the ideal tensile strength of a wide variety of covalent and ionic crystals with a single type of chemical bond with ZB, WZ, or RS structures from first-principles calculations, for which n_{AB}, d_{AB} and S_{hkl} are already known or can be calculated from the experimental values of the lattice parameters (Guo et al., 2009). Three parameters, C, m, and k, in Eqn. 3 can be deduced using the Levenberg-Marquardt method (Levenberg, 1944; Marquardt, 1963) by fitting Eqn. 3 with the crystal tensile strength values from first-principles calculations, leading to,

$$\sigma_{hkl}^{theor}(Pa) = 6.6\times10^{-10}S_{hkl}d_{AB}^{-1.32}\exp(3.7n_{AB}) \tag{4}$$

and

$$F_{AB}^{theor}(N) = 6.6\times10^{-10}d_{AB}^{-1.32}\exp(3.7n_{AB}) \tag{5}$$

The square of correlation coefficient R^2 is 0.996 with the mean absolute fractional deviation of ~7%, indicating that Eqn. 4 and 5 are accurate enough to estimate σ_{hkl} and F_{AB}.

Up to now, we are considering two bonding atoms, A and B, with totally 8 valence electrons. The simple formula for tensile unbinding force should be valid for complicate crystals, such as β–Si_3N_4, a-quartz, and a–Al_2O_3, where the total valence electrons of two bonding atoms

are more than 8. The chemical bonds in these crystals are typical two-electron bond. β–Si_3N_4 and *a*-quartz follow the *8-N* rule of structure, where *N* is the valence electron of an atom and *8-N* is the corresponding coordination number. Since there are one pair of non-bonding electrons for N in β–Si_3N_4 and two pairs of non-bonding electrons for O in β-quartz, n_N and n_O are both equal to 1. In *a*–Al_2O_3, The coordination number for Al and O are 6 and 4, respectively, leading to n_{Al} of 0.5 and n_O of 1.5. It is then straight forward to calculate the tensile unbinding force (bond strength) with Eqn. 5 for these crystals.

3. Results and discussions

In this section, we will start with the calculation of bond strength in chosen types of materials to understand the relationship of bond strength and crystal structure as well as to trace the relations between the macroscopic properties and bond strength. We will end this section with the bond strength calculations for some low-dimensional materials, such as graphene, h-BN sheet, and SWNT, to demonstrate the effectiveness of our semi-empirical quantification model to these systems.

3.1 IV-A semiconductors

The IV-A semiconductors belong to the family of A^NB^{8-N} semiconductors which have similar structures under normal conditions and follow similar phase transition rules under high pressure (Mujica et al., 2003). The procedure presented next can easily be applied to other members of A^NB^{8-N} semiconductors.The stable phases of the IV-A materials are graphite, diamond structured Si, Ge, and Sn, and a huge variety of polytypic forms of SiC with comparable energies such as 3C, 2H, 4H, and 6H. The phase transitions of these materials have been itemized previously with fifteen types of crystal structures for IV-A materials (Mujica et al., 2003). ZB, WZ, and RS structures are shown in Figure 1. The other 12 structures are summarized in Figure 2 with the coordination states of the atoms marked. ZB, WZ, RS, graphite, and sh (simple hexagonal) are simple with the marked directions parallel to the axes of broken bonds. Tensile strength can be calculated for materials crystallized in these structures in addition to bond strength.

Several points need to be mentioned for these complicated structures before we discuss the calculation results. Firstly, we give the hexagonal representation instead of the simple rhombohedral representation for r8 structure to show the structure more clearly. Secondly, Si atoms in Imma structure are eight-fold coordinated while Ge atoms in the same structure of are six-fold coordinated (Figure 2f). Thirdly, there are two types of coordination states in the most complicated structure Cmca, although these atoms are identical. We denote the ten-fold coordinated atoms located at 8d sites with white spheres, and the eleven-fold coordinated atoms at 8f sites with gray spheres, as shown in Figure 2g.

The lattice parameters and the calculated bond strengths are listed in Table I. Except the sh-Si and sh-Ge, the arithmetic average of the bond length are given in Table I for structures with different bond lengths. The bond strength of graphite, diamond, lonsdaleite, ZB-Si, WZ-Si, ZB-Ge, ZB-Sn, and ZB-SiC can be referred to our recent publication (Guo et al., 2009). The bond strength of the IV-A materials as a function of bond length is presented in Figure 3. The tensile unbinding forces are unambiguously grouped by distinct n_{AB} values of 0.943, 0.707, 0.471, 0.354, 0.269, and 0.236, respectively (from top to bottom). As n_{AB} reflects the coordination states, a lower value means a higher coordination number. Bond strength of sequential structures appearing along the pressure induced phase transitions will leap from

the higher line to the next higher one. For instance, the experimental phase transition sequence of Si under compression is ZB-Si (n_{AB}=0.707) → β-Sn (0.471) → (Imma→sh) (0.354) → Cmca (0.269) → (hcp→fcc) (0.236). In Figure 3, the bond strength in the same line decreases from left to right in the sequence of C-C, Si-C, Si-Si, Ge-Ge, and Sn-Sn except in the line of n_{AB}=0.269 where the order for Si-Si and Ge-Ge is reversed. The bond strengths of Si-Si and Ge-Ge on other lines are not as distinguishable as those of other bonds. Such an anomaly can be explained by the experimental facts that the radii difference of Si and Ge is not so significant as other elements (r_C=0.062 Å, r_{Si}=1.068 Å, r_{Ge}=1.090 Å, r_{Sn}=1.240 Å). Alternatively, the high transition pressure makes the bond length of Ge comparable to that of Si or even shorter, reminiscent of Cmca (n_{AB}=0.269). Briefly, the bond strength of the chemical bond in this type of materials is determined by the coordination number: the lower the coordination number, the higher the bond strength.

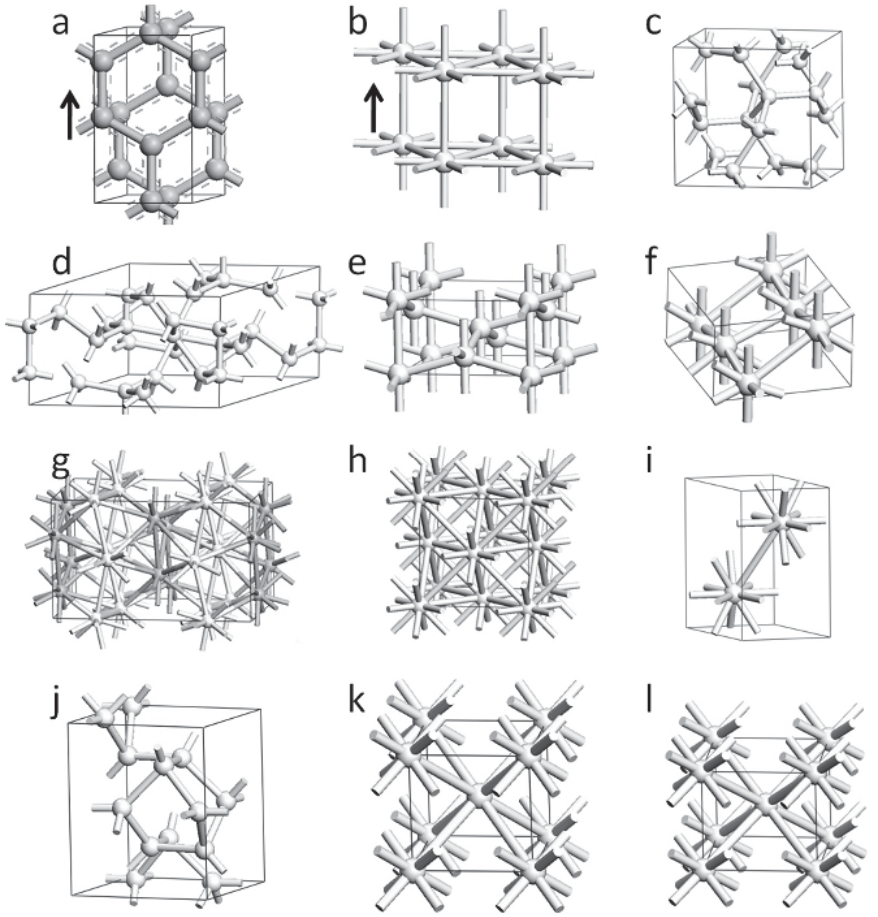

Fig. 2. Crystal structures of IV-A compounds without those in Figure 1. a) Graphite, b) sh, c) bc8, d) r8-h, e) β-Sn, f) Imma, g) Cmca, h) fcc, i) hcp, j) st12, k) bcc, and l) bct.

Bond	Crystal	Space Group	a (Å)	b (Å)	c (Å)	d (Å)	n_A	n_B	n_{AB}	F_{AB} (nN)
Si-Si	bc8	$Ia\bar{3}$	6.636			2.370	1	1	0.707	2.89
Si-Si	r8	$R\bar{3}$	9.125		5.447	2.319	1	1	0.707	2.98
Si-Si	β-Sn	$I4_1/amd$	4.686		2.585	2.475	0.667	0.667	0.471	1.14
Si-Si	sh	$P6/mmm$	2.549		2.383	2.549	0.5	0.5	0.354	0.71
						2.383	0.5	0.5	0.354	0.78
Si-Si	Imma	$Imma$	4.737	4.502	2.55	2.462	0.5	0.5	0.354	0.74
Si-Si	Cmca	$Cmca$	8.024	4.796	4.776	2.491	0.4	0.364	0.269	0.54
Si-Si	fcc	$Fm\bar{3}m$	3.34			2.362	0.333	0.333	0.236	0.51
Si-Si	hcp	$P6_3/mmc$	2.404		4.063	2.437	0.333	0.333	0.236	0.49
Ge-Ge	st12	$P4_32_12$	5.93		6.98	2.485	1	1	0.707	2.72
Ge-Ge	bc8	$Ia\bar{3}$	6.658			2.393	1	1	0.707	2.85
Ge-Ge	Imma	$Imma$	4.931	4.913	2.594	2.562	0.667	0.667	0.471	1.09
Ge-Ge	β-Sn	$I4_1/amd$	4.959		2.746	2.631	0.667	0.667	0.471	1.05
Ge-Ge	sh	$P6/mmm$	2.657		2.556	2.657	0.5	0.5	0.354	0.67
						2.556	0.5	0.5	0.354	0.71
Ge-Ge	Cmca	$Cmca$	7.886	4.656	4.667	2.430	0.4	0.364	0.269	0.55
Ge-Ge	hcp	$P6_3/mmc$	2.776		4.573	2.793	0.333	0.333	0.236	0.41
Sn-Sn	β-Sn	$I4_1/amd$	5.833		3.182	3.076	0.667	0.667	0.471	0.86
Sn-Sn	bcc	$Im\bar{3}m$	3.287			2.847	0.5	0.5	0.354	0.61
Sn-Sn	bct	$I4/mmm$	3.7		3.37	3.112	0.5	0.5	0.354	0.55
Si-C	4H	$P6_3mc$	3.079		10.073	1.894	1	1	0.707	3.89
Si-C	RS	$Fm\bar{3}m$	4.001			2.001	0.667	0.667	0.471	1.51

Table 1. Lattice parameters and bond strength of IV-A semiconductors.

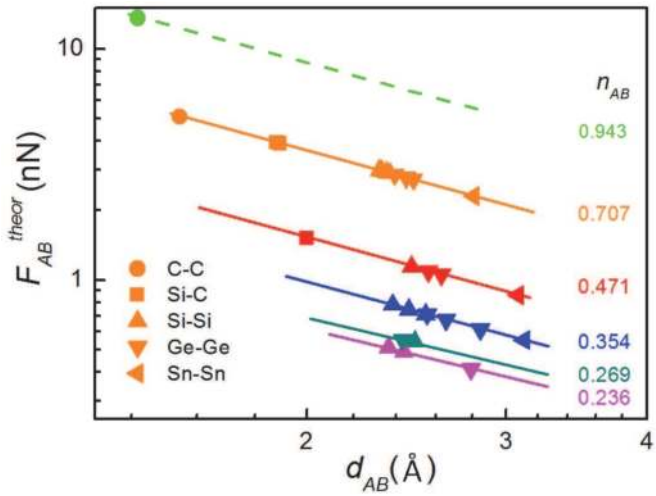

Fig. 3. Bond strength F_{AB}^{theor} vs. d_{AB} for IV-A compounds.

3.2 $A^N B^{8-N}$ ionic crystals

Our simple model for chemical bond strength can easily be applied to ionic crystals, just like the above considered pure covalent and polar covalent A^NB^{8-N} materials (Guo et al., 2009). The elemental combinations of IA-VIIA, IB-VIIA, and IIA (except Be)-VIA tend to form ionic crystals. The typical structures of ionic A^NB^{8-N} materials are RS and CsCl. ZB and WZ structures are also founded for some IB-VIIA crystals (Shindo et al., 1965). These four structures have been presented in Figure 1 and 2. Other structures, such as $R\bar{3}m$ (H) (Hull & Keen, 1994), P3m1 (Sakuma, 1988), P4/nmm (Liu, 1971), P21/m and Cmcm (Hull & Keen, 1999), can also be found in I-VIIA and IIA-VIA compounds and are shown in Figure 4. The concrete coordination state of each atom in these five structures is clearly shown. The distance between the two neighboring iodine atoms in P3m1-structured CuI is 4.353 Å. Consequently, this compound has a lamellar structure, significantly different from other dense structures.

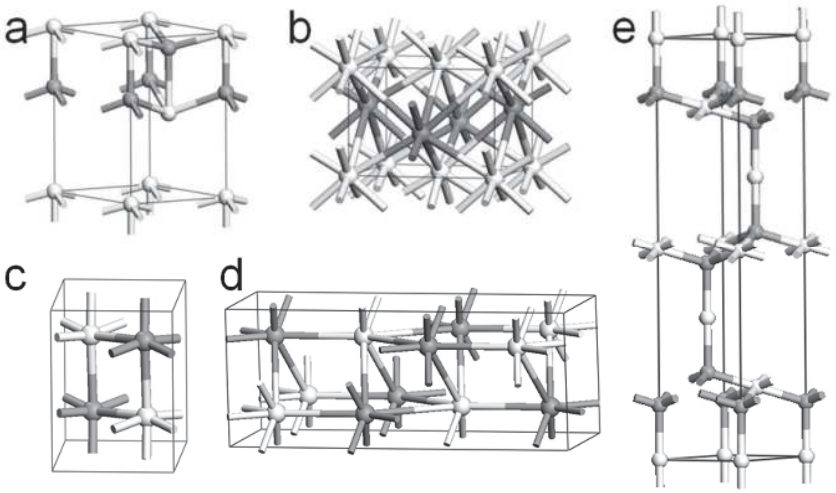

Fig. 4. Crystal structures of ionic *AB* compounds. a) P3m1, b) P4/nmm, c) $P2_1/m$, d) Cmcm, and e) $R\bar{3}m$.

In our previous work, the bond strength and uniaxial tensile strength of ten types of rocksalt structured compounds has been calculated (Guo et al., 2009). Crystal parameters and calculated bond strength of other ionic AB compounds are shown in Table 2. For the high pressure phases, the lattice parameters are given under compression. For the monoclinic structures of $P2_1/m$-structured AgCl, AgBr and AgI, β angles are 98.4°, 95.9°, and 98.4°, respectively. The unbinding tensile force versus bond length for I-VIIA and IIA-VIA compounds listed in Table 2 together with those given in previous work is shown in Figure 5. The bond strength of seventy six chemical bonds locates on seven parallel lines from top to the bottom with decreasing n_{AB} values.

3.3 III-VI crystals

Next step is to treat complicate crystals of A_mB_n with our semi-empirical quantification model of bond strength. We have discussed the most familiar compounds of β–Si_3N_4, *a*-

quartz, and a–Al_2O_3 in **Section 2**. The material members in this group are tremendous. Here only typical materials with the chemical composition of A_2B_3 (IIIA-VIA) are chosen for a demonstration. The crystal structures of the compounds as shown in Figure 6 are so complicated that sometimes identical atoms in the same structure have different coordination numbers. The nominal bonding valence electrons of atoms with lower electronegativity are equal to the numbers of outmost electrons, while the determination of the nominal bonding valence electrons of atoms with greater electronegativity is usually challenging.

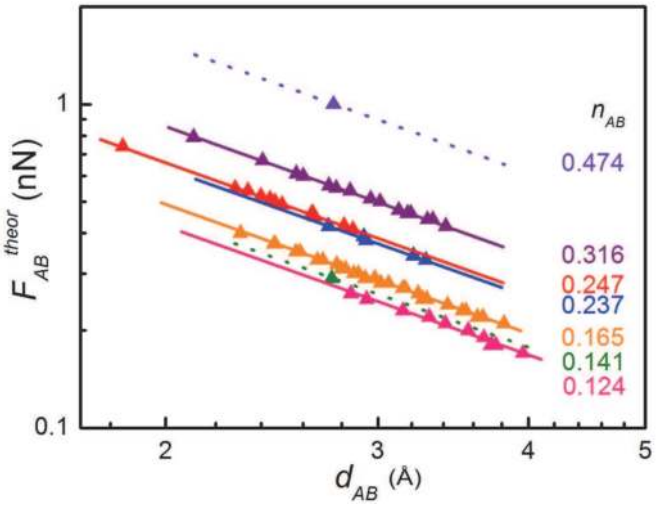

Fig. 5. Bond strength $F_{AB}{}^{theor}$ vs. d_{AB} for ionic AB compounds.

For B_2O_3 of $P3_121$ and B_2S_3 of lamellar $P2_1/c$, all B atoms are three-fold coordinated with O (S) atoms which are bonded to two B atoms. Considering the sp hybridization character of O atoms, the bonding valence electrons of O atoms are set to two. The situation differs from the $Cmc2$-structured B_2O_3 where B atoms are four-fold coordinated (Prewitt & Shannon, 1968). In this structure, one third of the O atoms are two-fold coordinated and the other two thirds are three-fold coordinated. For the three-fold coordinated O atoms, the nominal bonding valence electrons number is set to four due to the sp^2 hybridized orbital. While for the two-fold coordinated O atoms, only two nominal valence electrons are considered in bonding states and the other four stay at non-bonding states. In the case of Al_2S_3 with $P6_1$ symmetry, one fourth of Al atoms are six-fold coordinated (Al_{VI}) and other three fourths are four-fold coordinated (Al_{IV}), and all S atoms are three-fold coordinated with two Al_{VI} atoms and one Al_{IV} atom (Krebs et al., 1993).

Next structure is C_c for Ga_2Se_3 where Ga atoms are four-fold coordinated, one-third of Se atoms are two-fold coordinated and the other two thirds are three-fold coordinated with the nominal bonding valence electrons of 2 and 4, respectively (Lübbers & Leute, 1982). For In_2O_3 with $R\bar{3}c$ symmetry, the coordination number of In and O atoms are six and four, respectively (Prewitt et al., 1969). The $C2/m$-structured Ga_2O_3 is even more complicated(Ahman et al., 1996). Half of the Ga atoms are four-fold coordinated (Ga_{IV}) while the others six-fold coordinated (Ga_{VI}). O atoms in this structure are rather

complicated: one third of O atoms are four-fold coordinated to three Ga_{VI} atoms and one Ga_{IV} atom, another one third are three-fold coordinated to two Ga_{VI} atoms and one Ga_{IV} atom, and the last one third are three-fold coordinated to one Ga_{VI} atoms and two Ga_{IV} atom.
The lattice parameters, bond lengths, and bond strength are listed in Table 3. Most of the chemical bonds are two-electron bond. The bond strength versus bond length for these A_2B_3 and A_3B_4 compounds are shown in Figure 7 together with the data for Al_2O_3, β-C_3N_4 and β-Si_3N_4 from the previous work (Guo et al., 2009). Bond strength of the sixteen chemical bonds falls on seven parallel lines. Among all the two-electron bonds, the B-O bonds in $P3_121$-structured B_2O_3 exhibit the greatest unbinding tensile strength, even higher than that of C-C bond in diamond.

Bond	Crystal	Space group	a (Å)	b (Å)	c (Å)	d (Å)	n_A	n_B	n_{AB}	F_{AB} (nN)
Cu-F	ZB	$F\bar{4}3m$	4.255			1.842	0.25	1.75	0.247	0.74
Cu-Cl	ZB	$F\bar{4}3m$	5.406			2.341	0.25	1.75	0.247	0.54
Cu-Cl	WZ	$P63mc$	3.910		6.420	2.399	0.25	1.75	0.247	0.52
Cu-Cl	sc16	$Pa\bar{3}$	6.310			2.284	0.25	1.75	0.247	0.55
Cu-Cl	RS	$Fm\bar{3}m$	4.929			2.465	0.167	1.167	0.165	0.37
Cu-Br	ZBr	$F\bar{4}3m$	5.691			2.464	0.25	1.75	0.247	0.50
Cu-Br	WZ	$P63mc$	4.060		6.660	2.498	0.25	1.75	0.247	0.49
Cu-Br	sc16	$Pa\bar{3}$	6.738			2.442	0.25	1.75	0.247	0.51
Cu-Br	RS	$Fm\bar{3}m$	5.17			2.585	0.167	1.167	0.165	0.35
Cu-I	ZB	$F\bar{4}3m$	6.604			2.860	0.25	1.75	0.247	0.41
Cu-I	WZ	$P63mc$	4.310		7.090	2.659	0.25	1.75	0.247	0.45
Cu-I	P3m1	$P3m1$	4.279		7.17	2.644	0.25	1.75	0.247	0.46
Cu-I	$R\bar{3}m$	$R\bar{3}m$	4.155		20.48	2.648	0.25	1.75	0.247	0.46
Cu-I	RS	$Fm\bar{3}m$	6.121			3.061	0.167	1.167	0.165	0.28
Ag-F	RS	$Fm\bar{3}m$	4.920			2.460	0.167	1.167	0.165	0.37
Ag-Cl	RS	$Fm\bar{3}m$	5.546			2.773	0.167	1.167	0.165	0.32
Ag-Cl	$P2_1/m$	$P2_1/m$	3.587	3.992	5.307	2.700	0.167	1.167	0.165	0.33
Ag-Cl	Cmcm	$Cmcm$	3.399	10.124	4.023	2.747	0.143	1	0.141	0.29
Ag-Br	RS	$Fm\bar{3}m$	5.780			2.890	0.167	1.167	0.165	0.30
Ag-Br	$P2_1/m$	$P2_1/m$	3.821	3.98	5.513	2.798	0.167	1.167	0.165	0.31
Ag-I	ZB	$F\bar{4}3m$	6.499			2.814	0.25	1.75	0.247	0.42
Ag-I	WZ	$P63mc$	4.580		7.494	2.810	0.25	1.75	0.247	0.42
Ag-I	RS	$Fm\bar{3}m$	6.034			3.017	0.167	1.167	0.165	0.28
Ag-I	$P2_1/m$	$P2_1/m$	4.056	4.057	5.615	2.927	0.167	1.167	0.165	0.29
Ag-I	CsCl	$Pm\bar{3}m$	4.31			3.733	0.125	0.875	0.124	0.18
Li-Cl	RS	$Fm\bar{3}m$	5.130			2.565	0.167	1.167	0.165	0.35
Li-I	RS	$Fm\bar{3}m$	6.031			3.016	0.167	1.167	0.165	0.28
Li-I	NiAs	$P63/mmc$	4.48		7.26	3.160	0.167	1.167	0.165	0.27
K-F	RS	$Fm\bar{3}m$	5.344			2.672	0.167	1.167	0.165	0.33

K-Cl	CsCl	$Pm\bar{3}m$	3.634		3.147	0.125	0.875	0.124	0.23
K-Br	RS	$Fm\bar{3}m$	6.585		3.293	0.167	1.167	0.165	0.25
K-I	RS	$Fm\bar{3}m$	7.049		3.525	0.167	1.167	0.165	0.23
K-I	CsCl	$Pm\bar{3}m$	3.94		3.412	0.125	0.875	0.124	0.21
Rb-F	RS	$Fm\bar{3}m$	5.73		2.865	0.167	1.167	0.165	0.30
Rb-F	CsCl	$Pm\bar{3}m$	3.29		2.849	0.125	0.875	0.124	0.26
Rb-Cl	CsCl	$Pm\bar{3}m$	3.82		3.308	0.125	0.875	0.124	0.22
Rb-Br	RS	$Fm\bar{3}m$	6.855		3.428	0.167	1.167	0.165	0.24
Rb-Br	CsCl	$Pm\bar{3}m$	4.24		3.672	0.125	0.875	0.124	0.19
Rb-I	RS	$Fm\bar{3}m$	7.329		3.665	0.167	1.167	0.165	0.22
Rb-I	CsCl	$Pm\bar{3}m$	4.34		3.759	0.125	0.875	0.124	0.18
Cs-F	RS	$Fm\bar{3}m$	6.030		3.015	0.167	1.167	0.165	0.28
Cs-F	CsCl	$Pm\bar{3}m$	3.39		2.936	0.125	0.875	0.124	0.25
Cs-Cl	RS	$Fm\bar{3}m$	7.095		3.548	0.167	1.167	0.165	0.23
Cs-Cl	Cs	$Pm\bar{3}m$	4.115		3.564	0.125	0.875	0.124	0.20
Cs-Br	RS	$Fm\bar{3}m$	7.253		3.627	0.167	1.167	0.165	0.22
Cs-Br	CsCl	$Pm\bar{3}m$	4.296		3.720	0.125	0.875	0.124	0.18
Cs-I	RS	$Fm\bar{3}m$	7.631		3.816	0.167	1.167	0.165	0.21
Cs-I	CsCl	$Pm\bar{3}m$	4.568		3.956	0.125	0.875	0.124	0.17
Mg-Se	RS	$Fm\bar{3}m$	5.463		2.732	0.333	1	0.316	0.56
Mg-Te	WZ	$P63mc$	4.53	7.35	2.756	0.5	1.5	0.474	1.00
Ca-S	RS	$Fm\bar{3}m$	5.689		2.845	0.333	1	0.316	0.54
Ca-Se	RS	$Fm\bar{3}m$	5.916		2.958	0.333	1	0.316	0.51
Ca-Te	RS	$Fm\bar{3}m$	6.348		3.174	0.333	1	0.316	0.46
Ca-Te	CsCl	$Pm\bar{3}m$	3.387		2.933	0.25	0.75	0.237	0.38
Sr-O	RS	$Fm\bar{3}m$	5.134		2.567	0.333	1	0.316	0.61
Sr-S	RS	$Fm\bar{3}m$	6.023		3.012	0.333	1	0.316	0.50
Sr-S	CsCl	$Pm\bar{3}m$	3.372		2.920	0.25	0.75	0.237	0.39
Sr-Se	RS	$Fm\bar{3}m$	6.243		3.122	0.333	1	0.316	0.47
Sr-Te	RS	$Fm\bar{3}m$	6.659		3.330	0.333	1	0.316	0.44
Sr-Te	CsCl	$Pm\bar{3}m$	3.708		3.211	0.25	0.75	0.237	0.34
Ba-O	P4/nmm	$P4/nmm$	4.397	3.196	2.73	0.25	0.75	0.237	0.42
Ba-S	RS	$Fm\bar{3}m$	6.387		3.194	0.333	1	0.316	0.46
Ba-Se	RS	$Fm\bar{3}m$	6.593		3.297	0.333	1	0.316	0.44
Ba-Se	CsCl	$Pm\bar{3}m$	3.795		3.287	0.25	0.75	0.237	0.33
Ba-Te	Rs	$Fm\bar{3}m$	6.830		3.415	0.333	1	0.316	0.42

Table 2. Lattice parameters and bond strength of AB ionic compounds.

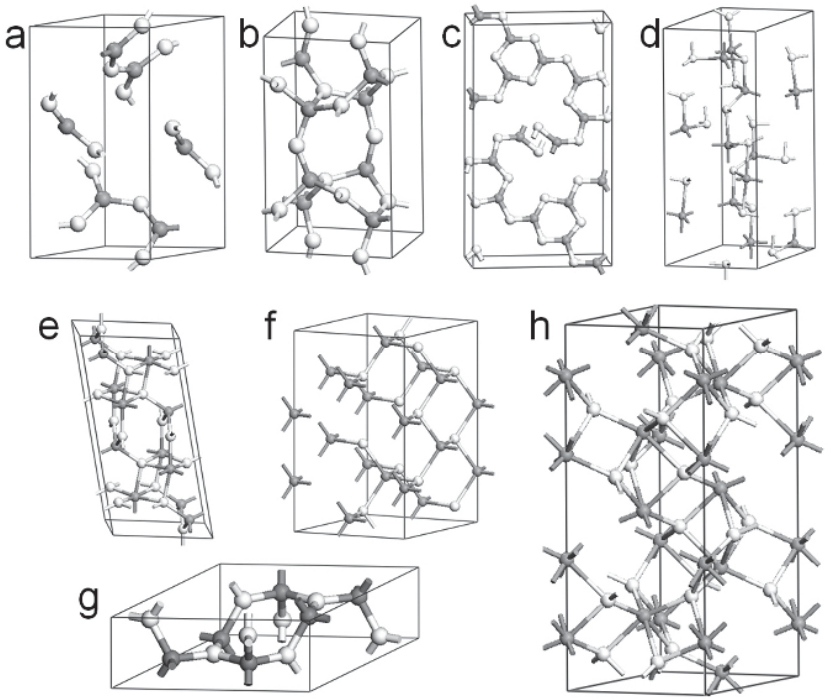

Fig. 6. Crystal structures of typical A_2B_3 and A_3B_4 compounds. White and gray spheres correspond to elements with higher and lower electronegativity, respectively. a) $P3_121$, b) $Cmc2_1$, c) $P2_1/c$, d) $P6_1$, e) C2/m, f) C_c, g) P3, and h) $R\bar{3}c$.

An extensive analysis of the A^NB^{8-N} materials will give twenty-four n_{AB} values, some of them has been shown in this work. The highest two are 0.943 and 0.856 occurring for three-fold coordinated C-C bond in graphite and three-fold coordinated B-N bond in h-BN, respectively. The common feature of these two bonds is more than two nominal valence electrons distributed on the bond, that is to say the bond order of them is higher than 1. The high bonded valence electron number makes them the strongest bonds to resist tensile force along the direction parallel to the axes of the bond. The next highest n_{AB} of 0.707 is from the four-fold coordinated two-electron bond where each atom contributes one valence electron to the bond, following by 0.643, 0.589, 0.530, 0.474, 0.471 and so on in the sequence. The lowest n_{AB} value is 0.124 corresponds to the Ag-I bond in the $Pm\bar{3}m$ -structured AgI.
Generally, lower coordination number results in higher bonded valence electron number, especially when the valence electron numbers of bonded atoms is the same. However, this argument does not hold when the valence electron numbers are different. For example, the Si atoms forming Si-Si bond in hcp- and fcc-structured Si are twelve-fold coordinated, which is the highest among the chemical bonds discussed above. The bonded valence electron number n_{AB} of these Si-Si bonds are 0.236, higher than the six-fold coordinated I-VIIA bonds (0.165), seven-fold coordinated I-VIIA bonds (0.141), and eight-fold coordinated I-VIIA bonds (0.124). It should be emphasized that the lines denoted with the same n_{AB} in different

figures are the same line, for instance, 0.707 in Figure 3 and 7, 0.474 in Figure 5 and 7. As long as the chemical bonds have the same n_{AB}, they will lie on the same line, and bond strength depends strictly on the bonded valence electron number n_{AB}. The relation of coordination number and n_{AB} therefore means that a lower coordination number corresponds to higher bond strength.

Crystal	Bond	Space group	a (Å)	b (Å)	c (Å)	d (Å)	n_A	n_B	n_{AB}	F_{AB} (nN)
B_2O_3	B-O	$P3_121$	4.336		8.340	1.368	1	1	0.707	5.97
B_2O_3	$B\text{-}O_{III}$	$Cmc2$	7.803	4.613	4.129	1.508	0.75	1.333	0.654	4.31
	$B\text{-}O_{II}$					1.373	0.75	1	0.6	4.00
B_2S_3	B-S	$P2_1/c$	4.039	10.722	18.620	1.794	1	1	0.707	4.18
Al_2S_3	$Al_V\text{-}S$	$P6_1$	6.491		17.169	2.376	0.6	1.333	0.547	1.59
	$Al_{IV}\text{-}S$					2.248	0.75	1.333	0.654	2.54
Ga_2O_3	$Ga_{VI}\text{-}O_{IV}$	$C2/m$	12.21	3.037	2.798	2.040	0.5	1.5	0.474	1.49
	$Ga_{VI}\text{-}O_{III}$					1.936	0.5	1.333	0.468	1.56
	$Ga_{IV}\text{-}O_{IV}$					1.863	0.75	1.5	0.671	3.47
	$Ga_{IV}\text{-}O_{III}$					1.833	0.75	1.333	0.654	3.33
Ga_2Se_3	$Ga\text{-}Se_{III}$	Cc	6.661	11.652	6.649	2.364	0.75	1.333	0.654	2.38
	$Ga\text{-}Se_{II}$					2.365	0.75	1	0.6	1.95
In_2O_3	In-O	$R\bar{3}c$	5.487		14.510	2.187	0.5	1.5	0.474	1.36

Table 3. Crystal parameters, bond length, and bond strength of A_2B_3 compounds.

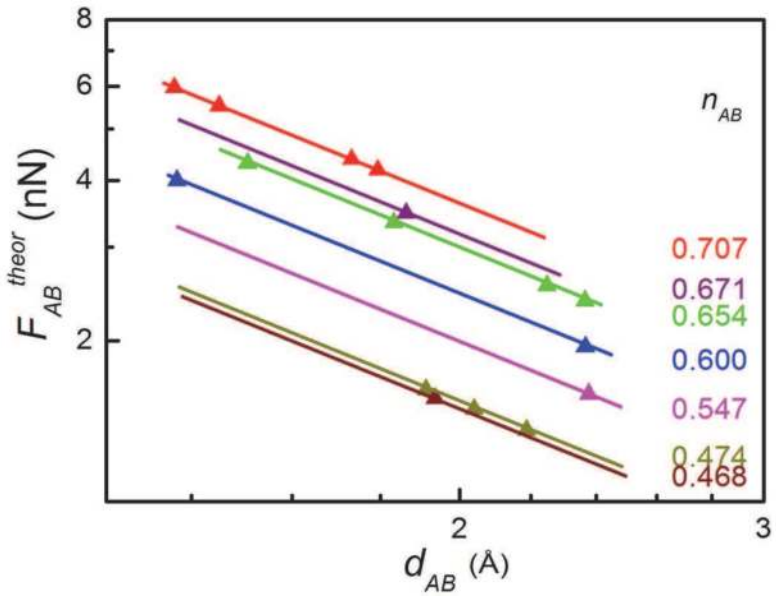

Fig. 7. Bond strength F_{AB}^{theor} vs. d_{AB} for typical A_2B_3 and A_3B_4 compounds

3.4 Low dimensional systems

We now apply our semi-empirical model to evaluate the theoretical tensile strength of the low dimensional systems, such as graphene, h-BN sheet, SWNT. As we mentioned before, the highest effective bonded valence electron numbers of 0.943 and 0.856 occur for three-fold coordinated C-C bond in graphite and three-fold coordinated B-N bond in h-BN, respectively. This is consistent with the argument that the sp^2 hybridized C-C bond in graphite is the strongest chemical bond (Coulson, 1952). Recently, graphene, a single atomic layer of graphite, has stirred enormous research interests owning to its exceptionally high crystallinity and electronic quality, as well as a fertile ground for applications (Geim & Novoselov, 2007). Experimentally, the mechanical properties of graphene have been identified with atomic force microscope (AFM) nanoindentation, giving a tensile strength of 130 GPa (Lee et al., 2008). Here we predict the theoretical tensile strength σ_{10}^{theor} of graphene in <*10*> direction using the present model as follows

$$\sigma_{10}^{theor} = S_{10}F_{cc} = \frac{F_{cc}}{\sqrt{3}d_{cc} \times \delta R} \tag{6}$$

where δR is the thickness of graphene taken as the interlayer separation 3.4 Å of graphite. F_{cc} and d_{cc} values are listed in Table 4 for graphene and other low dimensional systems. The theoretical tensile strength obtained is 162.7 GPa in the <*10*> direction, 20% higher than the experimental value.

Whilst graphene has a great application potential in microelectronics, hexagonal boron nitride (h-BN) sheets can find uses as an effective insulator in graphene based electronics. The mechanic properties of h-BN sheets have recently been investigated. With an elastic constant (E^{2D}) of 292 Nm^{-1}, a breaking strain of 0.22, and a thickness of 0.33 nm for a single atomic layer of h-BN (Song et al., 2010), the tensile strength can be deduce to be 97 GPa with the procedure suggested for graphene (Lee et al., 2008). Accordingly, the theoretical tensile strength of h-BN in the <*10*> direction can be calculated with our semi-empirical model, giving a value of 117 GPa, which is in good agreement with the experimental deduced value.

Carbon nanotube (CNT), with the same covalent sp^2 bonds formed between individual carbon atoms as graphen, is one of the strongest and stiffest materials. Direct tensile testing of individual tubes is challenging due to their small size (10 nm or less in diameter). There are several experimental efforts on the mechanical properties of CNT (Yu et al., 2000; Demczyk et al., 2002; Ding et al., 2006; Barber et al., 2005). However, the reported failure stress values display a large variance and are well below the theoretical predicted values in most cases (Ozaki et al., 2000; Mielke et al., 2004), which are attributed to the large number of defects presented on the nanotubes. Accurate measurements of tensile strength require high-quality CNT with well-defined sample parameters, as well as the elimination of measurement uncertainties. Notwithstanding, for zigzag single wall nanotube (SWNT), the theoretical tensile strength along the axial direction can be predicted with our simple model as,

$$\sigma_{axial}^{theor} = S_{axial}F_{AB} = \frac{nF_{AB}}{\pi[(\frac{D_{ep} + \delta R}{2})^2 - (\frac{D_{ep} - \delta R}{2})^2]} \tag{7}$$

where D_{ep} is the diameter of selected nanotube and n is the first index of the chiral vector (n, m) for nanotubes. The theoretical tensile strength of C (10, 0), SiC (10, 0), BN (10, 0), and AlN (10, 0) SWNTs are listed in Table 4.

Bond	Material	D_{ep} (Å)	D_{AB} (Å)	n_A	n_B	n_{AB}	F_{AB}^{theor} (nN)	σ_{theor} (GPa)
C-C	Graphene ⟨01⟩	–	1.419	1.333	1.333	0.943	13.6	162.7
B-N	h-BN sheet ⟨01⟩	–	1.446	1	1.667	0.857	9.65	117
C-C	C (10,0)	7.91	1.42	1.333	1.333	0.943	13.6	161.0
Si-C	SiC (10,0)	9.95	1.80	1.333	1.333	0.943	9.94	93.6
B-N	BN (10,0)	8.11	1.45	1	1.667	0.857	9.65	111.4
Al-N	AlN (10,0)	10.33	1.83	1	1.667	0.857	7.10	64.3

Table 4. Parameters, calculated bond strength, and tensile strength for selected low dimensional systems.

Before we end this section, there is one last point need to be mentioned regarding to the dependence of the tensile strength on the direction of the applied tensile stress. A tensile stress tilted away from the axis of a chemical bond would generate a shear component with respect to the bond, and we cannot perform the tensile strength calculation with Eqn. 3 under this circumstance. However, if the shear unbinding strength can be expressed, the ideal strength along any specific direction of a crystal will be accessible. Further studies are therefore highly expected.

4. Conclusion

The bond strength of a variety of chemical bonds are analysized with our semi-empirical unbinding tensile force model. This model proves to be valid for a wide selection of crystals, as well as low-dimensional materials such as graphene and nanotubes. In this model, the chemical bond strength, defined as the tensile unbinding force F_{AB}, can be calculated quantitatively in terms of the bond length d_{AB} and effective bonded valence electron number n_{AB}. It is demonstrated that the bond strength relies strongly on the crystal structure of a solid, in particular, the coordinated states of the bonded atoms. As a result, a chemcial bond formed by identical atom pair would have distinct bond strength in different crystal structures. For example, the the C-C bond strength in graphite is 2.67 times as high as that in diamonds. The definition of unbinding tensile strength provides a more intuitive and general representation of bond strength than those of cohensive energy for covalent crystals and lattice anergy for ionic crystals.

5. Acknowledgment

This work was supported by NSFC (Grant Nos. 50821001 and 91022029), by NBRPC (Grant No. 2011CB808205).

6. References

Ahman, J., Svensson, G. & Albertsson, J. (1996). A reinvestigation of beta-gallium oxide. *Acta Crystallographica Section C-Crystal Structure Communications*, Vol.52, No.6, pp. 1336-1338, ISSN 0108-2701

Barber, A. H., Andrews, R., Schadler, L. S. & Wagner, H. D. (2005). On the tensile strength distribution of multiwalled carbon nanotubes. *Applied Physics Letters*, Vol.87, No.20, 203106, ISSN 0003-6951

Brown, I. D. & Shannon, R. D. (1973). Empirical bond-strength bond-length curves for oxide. *Acta Crystallographica Section A*, Vol. 29, No.5, pp. 266-282, ISSN 0108-7673

Coulson, C. A. (1950). *Valence*, Oxford University Press, Oxford.

Demczyk, B. G., Wang, Y. M., Cumings, J., Hetman, M., Han, W., Zettl, A. & Ritchie, R. O. (2002). Direct mechanical measurement of the tensile strength and elastic modulus of multiwalled carbon nanotubes. *Materials Science and Engineering a-Structural Materials Properties Microstructure and Processing*, Vol.334, No.1-2, pp. 173-178, ISSN 0921-5093

Ding, W., Calabri, L., Kohlhaas, K. M., Chen, X., Dikin, D. A. & Ruoff, R. S. (2007). Modulus, fracture strength, and brittle vs. plastic response of the outer shell of arc-grown multi-walled carbon nanotubes. *Experimental Mechanics*, Vol.47, No.1, pp. 25-36, ISSN 0014-4851

Gao, F. M., He, J. L., Wu, E. D., Liu, S. M., Yu, D. L., Li, D. C., Zhang, S. Y. & Tian, Y. J. (2003). Hardness of covalent crystals. *Physical Review Letters*, Vol.91, No.1, 015502, ISSN 0031-9007

Geim, A. K. & Novoselov, K. S. (2007). The rise of graphene. *Nature Materials*, Vol.6, No.3, pp. 183-191, ISSN 1476-1122

Gibbs, G. V., Hill, F. C., Boisen, M. B. & Downs, R. T. (1998). Power law relationships between bond length, bond strength and electron density distributions. *Physics and Chemistry of Minerals*, Vol.25, No.8, pp. 585-590, ISSN 0342-1791

Gibbs, G. V., Rosso, K. M., Cox, D. F. & Boisen, M. B. (2003). A physical basis for Pauling's definition of bond strength. *Physics and Chemistry of Minerals*, Vol.30, No.5, pp. 317-320, ISSN 0342-1791

Guo, X. J., Wang, L. M., Xu, B., Liu, Z. Y., Yu, D. L., He, J. L., Wang, H. T. & Tian, Y. J. (2009). Unbinding force of chemical bonds and tensile strength in strong crystals. *Journal of Physics-Condensed Matter*, Vol.21, No.48, 485405, ISSN 0953-8984

He, J. L., Wu, E. D., Wang, H. T., Liu, R. P. & Tian, Y. J. (2005). Ionicities of boron-boron bonds in B-12 icosahedra. *Physical Review Letters*, Vol.94, No.1, 101906, ISSN 0031-9007

Hull, S. & Keen, D. A. (1994). High-pressure polymorphism of the copper(I) halides – a neutron-diffraction study to ~10 GPa. *Physical Review B*, Vol.50, No.9, pp. 5868-5885, ISSN 0163-1829

Hull, S. & Keen, D. A. (1999). Pressure-induced phase transitions in AgCl, AgBr, and AgI. *Physical Review B*, Vol.59, No.2, pp. 750-761, ISSN 0163-1829

Hultgren, R. (1932). Equivalent chemical bonds formed by s, p, and d eigenfunctions. *Physical Review*, Vol.40, No.6, pp. 0891-0907, ISSN 0031-899X

Kittle, C. (2004). *Introduction to Solid State Physics*, Wiley, ISBN 978-0471415268, New York.

Krebs, B., Schiemann, A. & Lage, M. (1993). Synthesis and crystal-structure of a novel hexagonal modification of Al_2S_3 with 5-coordinated aluninum. *Zeitschrift Fur Anorganische Und Allgemeine Chemie*, Vol.619, No.6, pp. 983-988, ISSN 0044-2313

Lee, C., Wei, X. D., Kysar, J. W. & Hone, J. (2008). Measurement of the elastic properties and intrinsic strength of monolayer graphene. *Science*, Vol.321, No.5887, pp. 385-388, ISSN 0036-8075

Levenberg, K. (1944). A method for the solution of certain non-linear problems in least squares. *Quarterly of Applied Mathematics* Vol.2, pp. 164-168, ISSN 0033-569X

Li, K. Y., Wang, X. T., Zhang, F. F. & Xue, D. F. (2008). Electronegativity identification of novel superhard materials. *Physical Review Letters*, Vol.100, No.23, 235504, ISSN 0031-9007

Liu, L. G. (1971). Dense modification of BaO and its crystal structure. *Journal of Applied Physics*, Vol.42, No.10, pp. 3702-3704, ISSN 0021-8979

Lübbers, D. & Leute, V. (1982). The crystal structure of β-Ga_2Se_3. *Journal of Solid State Chemistry*, Vol.43, No.3, pp. 339-345, ISSN 0022-4596

Marquardt, D. W. (1963). An algorithm for least-square estimation of nonlinear parameters. *Journal of the Society for Industrial and Applied Mathematics*, Vol.11, No.2, pp. 431-441, ISSN 0368-4245

Mielke, S. L., Troya, D., Zhang, S., Li, J. L., Xiao, S. P., Car, R., Ruoff, R. S., Schatz, G. C. & Belytschko, T. (2004). The role of vacancy defects and holes in the fracture of carbon nanotubes. *Chemical Physics Letters*, Vol.390, No.4-6, pp. 413-420, ISSN 0009-2614

Mujica, A., Rubio, A., Munoz, A. & Needs, R. J. (2003). High-pressure phases of group-IV, III-V, and II-VI compounds. *Reviews of Modern Physics*, Vol.75, No.3, pp. 863-912, ISSN 0034-6861

Mulliken, R. S. (1955). Electronic population analysis on LCAO-MO molecular wave functions. *Journal of Chemical Physics*, Vol.23, No.10, pp. 1833-1840, ISSN 0021-9606

Ozaki, T., Iwasa, Y. & Mitani, T. (2000). Stiffness of single-walled carbon nanotubes under large strain. *Physical Review Letters*, Vol.84, No.8, pp. 1712-1715, ISSN 0031-9007

Pauling, L. (1929). The principles determining the structure of complex ionic crystals. *Journal of the American Chemical Society*, Vol.51, No.4, pp. 1010-1026, ISSN 0002-7863

Prewitt, C. T. & Shannon, R. D. (1968). Crystal structure of a high-pressure form of B_2O_3. *Acta Crystallographica Section B-Structural Crystallography and Crystal Chemistry*, Vol.24, No.6, pp. 869-874, ISSN 0108-7681

Prewitt, C. T., Shannon, R. D., Rogers, D. B. & Sleight, A. W. (1969). C rare earth oxide-corundum transition and crystal chemisty of oxides having the corundum structure. *Inorganic Chemistry*, Vol.8, No.9, pp. 1985-1993, ISSN 0020-1669

Roundy, D., Krenn, C. R., Cohen, M. L. & Morris, J. W. (1999). Ideal shear strengths of fcc aluminum and copper. *Physical Review Letters*, Vol.82, No.13, pp. 2713-2716, ISSN 0031-9007

Sakuma, T. (1988). Crystal-structure of β-CuI. *Journal of the Physical Society of Japan*, Vol.57, No.2, pp. 565-569, ISSN 0031-9015

Segall, M. D., Shah, R., Pickard, C. J. & Payne, M. C. (1996). Population analysis of plane-wave electronic structure calculations of bulk materials. *Physical Review B*, Vol.54, No.23, pp. 16317-16320, ISSN 0163-1829

Shindo, K., Morita, A. & Kamimura, H. (1965). Spin-orbit coupling in ionic crystal with zincblende and wurtzite structures. *Journal of the Physical Society of Japan*, Vol.20, No.11, pp. 2054-2059, ISSN 0031-9015

Simunek, A. & Vackar, J. (2006). Hardness of covalent and ionic crystals: First-principle calculations. *Physical Review Letters*, Vol.96, No.8, 085501, ISSN 0031-9007

Song, L., Ci, L. J., Lu, H., Sorokin, P. B., Jin, C. H., Ni, J., Kvashnin, A. G., Kvashnin, D. G., Lou, J., Yakobson, B. I. & Ajayan, P. M. (2010). Large scale growth and characterization of atomic hexagonal boron nitride layers. *Nano Letters*, Vol.10, No.8, pp. 3209-3215, ISSN 1530-6984

Yu, M. F., Lourie, O., Dyer, M. J., Moloni, K., Kelly, T. F. & Ruoff, R. S. (2000). Strength and breaking mechanism of multiwalled carbon nanotubes under tensile load. *Science*, Vol.287, No.5453, pp. 637-640, ISSN 0036-8075

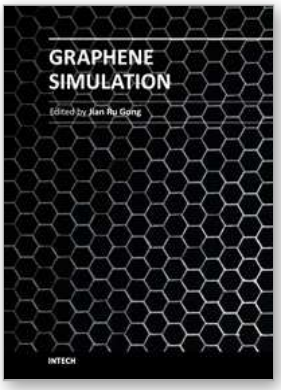

Graphene Simulation

Edited by Prof. Jian Gong

ISBN 978-953-307-556-3
Hard cover, 376 pages
Publisher InTech
Published online 01, August, 2011
Published in print edition August, 2011

Graphene, a conceptually new class of materials in condensed-matter physics, has been the interest of many theoretical studies due to the extraordinary thermal, mechanical and electrical properties for a long time. This book is a collection of the recent theoretical work on graphene from many experts, and will help readers to have a thorough and deep understanding in this fast developing field.

InTech Europe
University Campus STeP Ri
Slavka Krautzeka 83/A
51000 Rijeka, Croatia
Phone: +385 (51) 770 447
Fax: +385 (51) 686 166
www.intechopen.com

InTech China
Unit 405, Office Block, Hotel Equatorial Shanghai
No.65, Yan An Road (West), Shanghai, 200040, China
中国上海市延安西路65号上海国际贵都大饭店办公楼405单元
Phone: +86-21-62489820
Fax: +86-21-62489821